CZU: 538.9 DOI: 10.36120/2587-3644.v8i2.124-135

LASER ABLATION APPLIED FOR SYNTHESIS OF THIN FILMS GaSb‹Fe› AND GaSb‹Mn›

Mariana OSIAC, University of Craiova, Romania
Igor POSTOLACHI, Tiraspol State University, Moldova

Abstract. Knowledge of the physics properties of Gallium Antimonide (*GaSb*) is important because of the increasing application of *GaSb* in many optical and electronics applications. X-ray diffraction and electron micrographic analyses showed that *GaSb‹Fe›* and *GaSb‹Mn›* eutectic composites doped with 0.1% and 2,0% Fe atoms are perfective. The density of inclusion in *GaSb‹Fe›* composites increased about two times than undoped samples. Iron-doped gallium antimony thin films at concentrations in the range (0.1÷2.0) atomic% were obtained by laser ablation.

Key words: Gallium Antimonide (*GaSb*), *GaSb‹Fe›* and *GaSb‹Mn›*, laser ablation, X-ray diffraction - XRD.

ABLAȚIE LASER APLICATA PENTRU SINTEZA FILMELOR SUBȚIRI DE GaSb‹Fe› ȘI GaSb‹Mn›

Abstract. Cunoașterea proprietăților fizice ale antimonidului de galiu (*GaSb*) este importantă datorită implementării crescânde a *GaSb* în multe aplicații optice și electronice. Difracția cu raze X și analizele micrografice electronice au arătat că compozitele eutectice *GaSb ‹Fe›* și *GaSb ‹Mn›* dopate cu 0,1% și 2,0% atomi de Fe sunt perfective. Densitatea incluziunii în compozitele *GaSb ‹Fe›* a crescut de aproximativ două ori decât în mostrele nedopate. Pelicule subțiri de antimoniu de galiu dopate cu fier la concentrații în intervalul (0,1 ÷ 2,0) % atomare, au fost obținute prin ablație laser.

Cuvinte cheie: Antimonid de galiu (*GaSb*), *GaSb ‹Fe›* și *GaSb ‹Mn›*, ablație laser, difracție cu raze X - XRD.

Introduction

Gallium Antimonide (*GaSb*) belongs to antimonide compound semiconductors family which have a smaller band gap among $A^{III}B^{V}$ semiconductors, making them suitable for optoelectronic devices operated in the infrared region and electronic devices in the wavelength range 1÷5 μm [6, 10, 14-17, 20-22, 25-26, 39].

Crystals of *GaSb* has an energy band gap of 0,70 *eV* (1,77 μm) at room temperature and 0,81 *eV* (1,53 μm) at 4*K* [37]. *GaSb*-based devices such as near infrared photodetectors, resonant tunnelling structure, laser diodes and other quantum devices have been previously reported [1-4,7-9, 23-24, 27-28, 31-33]. *GaSb* based structures have shown potentiality for applications in laser diodes with low threshold voltage [18, 29], photodetectors with high quantum efficiency [7, 19, 32], high frequency devices [1, 8], superlattices with tailored optical and transport characteristics [13, 39], booster cells in tandem solar cell arrangements for improved efficiency of photovoltaic cells and high efficiency thermophotovoltaic (TPV) cells [3, 13]. *GaSb*-based devices are promising candidates for variety of military and civil applications in the 2-5 and 8-14 μm regimes: To mention a few, infrared (IR) imaging sensors for missile and surveillance systems (focal plane arrays), fire detection and monitoring environmental pollution. *GaSb* has also proved to be a model material for several basic studies [11]. Because of the band

structural properties, *GaSb* has proved to be an ideal material for studying the Auger recombination processes [5].

Initial synthesis of crystals of GaSb doped with Fe and Mn

Due to the fact that according to its physical properties *GaSb* strongly resembles the materials in group IV of the periodic table, methods similar to those used for the synthesis and growth of Si, Ge and $GaAs$ crystals were used for the synthesis and growth of $GaSb$.

The $GaSb$ compound is obtained by direct synthesis of primary elements of Ga, Sb. The peculiarities of obtaining the $GaSb$ compound are related to the way of interaction between the primary components among themselves and their melts with the surface of the container (ampoule) in which the material is synthesized. Ga melts at 29,8°C and is a material with a rather high boiling point temperature of 2230°C. In the temperature range between the melting and boiling points, the gallium antimony has a low sublimation rate, so that at the temperature $\sim 1300K$ the vapour pressure does not exceed 10^{-3} $mm\ Hg$. Ga having a low melting temperature in its liquid state moistens the surface of the optical quartz ampoule. The melting point of the antimony is 630,5°C and it boils at 1044°C. If the thermal regime of the antimony is technologically favourable for the synthesis of the $GaSb$ compound, then some difficulties arise due to the low chemical activity of the antimony with Ga. This particularity places certain requirements to the technology of obtaining the homogeneous compositional crystals.

The primary $GaSb$ compound was synthesized from elementary components Ga and Sb with 5N purity, taken in stoichiometric quantities. The quantity of the (Ga, Sb) alloy components and the (Fe, Mn) dopant was appreciated with the accuracy of $10^{-4}g$. The total quantity of the material for synthesis was 20-25 *g*. The material for synthesis was placed into quartz optic ampoules with thick walls of $(2 \div 3)mm$ and internal diameter of ~ 20 *mm*. After evacuating the air to the remaining pressure of 10^{-4} *mm Hg*, the ampoules were sealed. The process of evacuating the atmospheric air alternates with several cycles of "washing" with argon. At the pressure of the remaining gases of 10^{-4} *mm Hg*, the ampoules with the substance necessary to obtain the samples are hermetically sealed and welded at the quartz stick, through which the ampoule with the material is attached to the electromagnetic vibrator. In fig.1. a diagram of the furnace used for the synthesis of the *GaSb* compound is presented.

The oven is fixed on a movable support with the help of which the ampoule with the substance can occupy the position in the range angles of 0-90°. The furnace characteristics: maximum temperature $1020^{o}C$; the length of the thermal zone with temperature $900^{o}C$ was 28 *cm*; as a temperature sensor two thermocouples of Cromeli-

Alumeli type were used; the contacts of the thermocouple were fixed at the ends of the ampoule.

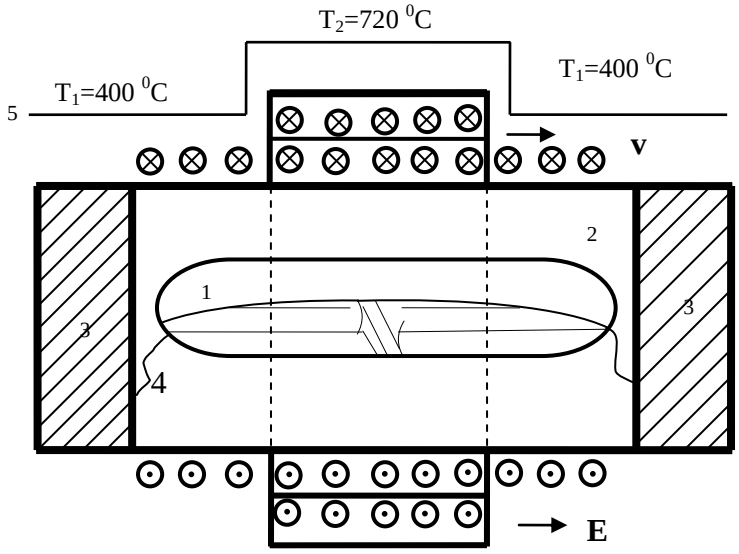

Figure 1. The technological installation for the synthesis of crystals

1 - GaSb ingot tube as a result of the synthesis process; **2** - electric oven;
3 - porous brick sheets; **4** - electromagnetic vibration mechanism;
5 - temperature diagram; **6** - mobile melting zone;
E - the intensity of the electric field; **v** - the speed of movement of the melted area.

The solidification temperature of the *GaSb* compound, according to the phase diagram, is 705,9^{o}C, so that in order to obtain mono-crystals the method of the molten area was chosen. In order to obtain crystalline substances with a strictly defined melting point, the polycrystalline substance is initially melted and then the melting temperature is slowly lowered below the melting point. The simplest are the methods in which the crystallization takes place as a result of gradual solidification of the melt at one end of the container (directional crystallization). In order to obtain crystals with a diameter of 20 *mm*, a requirement for the ablation process we can use vertical crystallization methods (Bridgman, Stockbarger, Kyropoulos).

The disadvantage of these methods is the contact of the melt with the walls of the container, which makes it difficult to grow a single crystal due to the formation of a large number of crystallization centers. This is especially true when the melt cleans the container walls well. To eliminate this phenomenon, the walls of the quartz ampoule were covered with soot. The Bridgman-Stockbarger method or the directional solidification method consists of the following, through a furnace with a different temperature distribution along the length, an ampoule with synthesized material is extracted (it is possible to use a fixed ampoule and a moving furnace). The ampoule has a sharp end to eliminate the formation of a large number of crystallization embryos. The crystallization by this method can take place when the ampoule is moved with the liquid

(molten) substance in the furnace from the high temperature region to the low temperature region. As a result, the crystallization starts at the bottom of the cone-shaped melting pot, and due to the geometric selection, a single crystal grows, which after the crystallization has the shape of the vessel.

Both experimental and theoretical studies show that in Bridgman's growth method, it is the appearance of convection currents from the melt that have a great influence on the quality of the grown crystal. Therefore, by controlling the convection currents, we can control the heat transfer and the mass in the melt and, therefore, the quality of the grown crystal.

Experimental studies have shown that flows in the melt can improve and affect the uniformity of the distribution of impurities in the grown crystal. On the one hand, the currents, which contribute to the mixing of impurities in the melt, increase the uniformity of the distribution. On the other hand, the melt currents transfer the impurity and are capable of disrupting the uniform distribution of the impurity in the grown crystals, creating areas where there is a local excess or lack of impurities. In this sense, the currents are harmful and must be effectively suppressed. Research has shown that the vibration flows in the melt are particularly harmful, because in such a flow the impurity is redistributed in an unpredictable way. To suppress the currents, furnaces must be used, with a stable stratification of the melting temperature gradient. It has been established that under terrestrial conditions, such a stable stratification is a constant gradient of the vertical temperature, oriented vertically upwards.

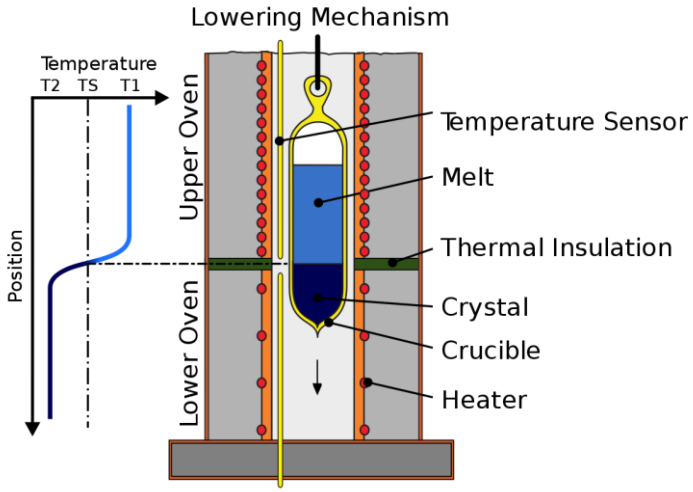

Figure 2. Instalation for growing the *GaSb*(*Fe, Mn*) crystals

The temperature in the upper area was stable, equal to 740^{o}C, and in the lower region the temperature was about 700^{o}C. The maximum speed of descending the ampoule was 5*mm*/*h*.

The degree of homogeneity of the (*Fe, Mn*) dopant distribution in mono- crystals was verified by the method of atomic emission spectra. The typical mono-crystals of *GaSb‹Fe›* grown through the zonal melting method are shown in Figure 3.

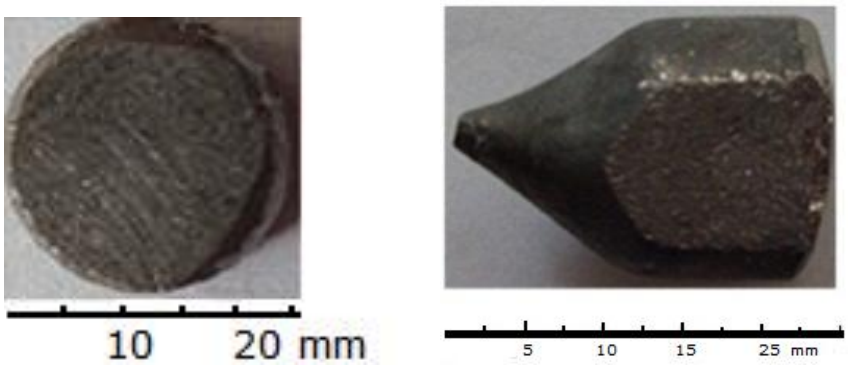

a) ***b)***

Figure 3. Sample photos, *GaSb‹Fe›* in 2 sections: (a - cross section); (b - longitudinal)

For the obtained materials, galvan-magnetic measurements were carried out on standard equipment in direct current regime. The density of current j_x in the sample, the potential difference (U_x) and the difference of potential between the Hal electrodes (U_y) and the electrodes for measurements of conductivity $\boldsymbol{\sigma}$, were recorded. The experimental data of the galvan-magnetic measurements showed that all the samples possess a major conductivity of type p. The concentration of gaps in the *GaSb*(*Fe*) and *GaSb*(*Mn*) samples has varied within the limits $2 \cdot 10^{17}\ cm^{-3}$ - $3 \cdot 10^{18}\ cm^{-3}$.

Obtaining of the thin films of GaSb doped with different concentrations of Fe and Mn, silica and antimony of arsenite by laser ablation Surelite II Nd: YAG

The deposits were made in a cylindrical stainless steel vacuum chamber (volume was about ~10*l*, height - 30 *cm*, diameter - 20 *cm*). The room was evacuated of the atmosphere at a pressure of about ~ 10-6 Torr. Argon (*Ar*) was introduced to deposit *GaSb* films in the chamber.

GaSb(*Fe, Mn*) platelets are placed on a XYZ support of micrometric precision. The metal support is electrically insulated through a ceramic block (alumina). The Si substrate is placed parallel to the target; the target-substrate distance can be adjusted in the range of 0,5 - 10 *cm*. For some experiments, the substrate was also rotated.

The laser ablation beam was incidentally oriented at 45 ° on the target surface, which enters the room through the window D of Fig. 4, with the help of the substrate placed on the hole C. For some experiments, the laser beam entered through port C, at an incidental angle of 45°, but in this case the substrate (rotating) support was placed on the D-hole, and the target was placed on a 45° support, while the target and substrate surfaces

were always parallel. In this case, the target was not rotated, but was moved in the *XY* plane with the micrometric stage.

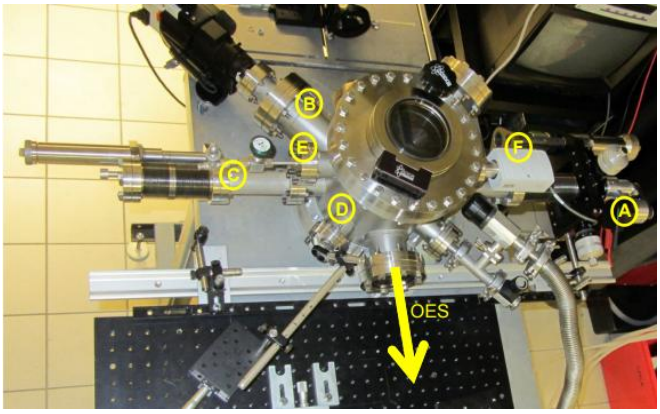

Figure 4. Vacuum chamber used for laser ablation

Figure 5 presents the main scheme of the chamber to obtain the *GaSb* films by laser ablation. The samples of *GaSb* or *GaSb* doped with *Fe* and *Mn* were fixed to the support and served as a target.

Laser radiation was focused on the surface of the (*GaSb*) target using the lens. The support along with the target were in rotational motion.

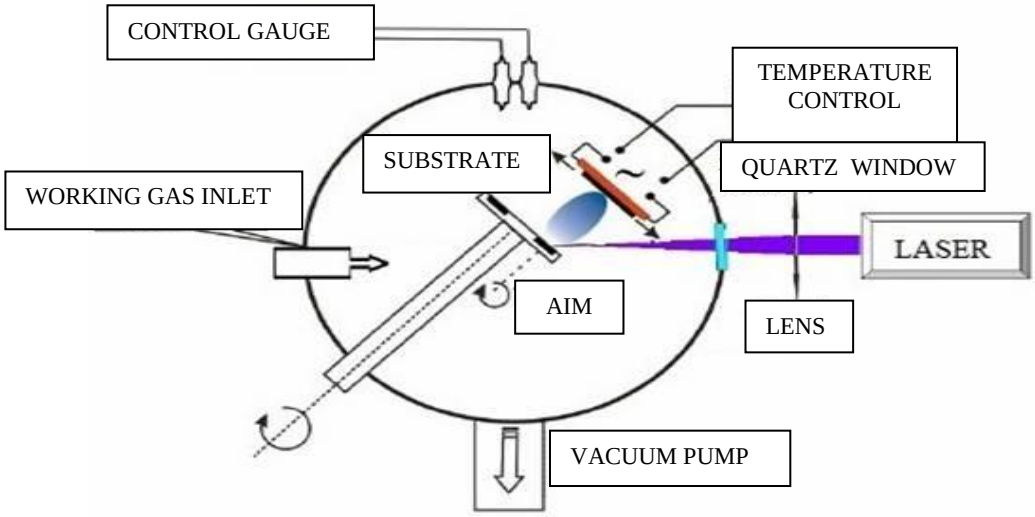

Figure 5. Main scheme of the camera for obtaining thin films of *GaSb* doped with *Fe* and *Mn* by laser ablation method

Under the action of laser photons a portion of the target substrate is evaporated and removed to the support. The Nd: YAG (Surelite III-10) laser changed with nanoseconds was used as a photon source. The nanosecond laser can generate four distinct wavelengths at 1064, 532, 355 and 266 *nm*, with maximum energy / pulse of 900, 430, 170 and 110 *mJ* respectively, at a frequency of 10 *Hz*. The pulse duration is in the range of 3-6 *ns* (depending on the harmonics used), and the beam diameter is ~ 9 *mm* (for a divergence of 0,5 *mrad*). The optical scheme of this laser is shown in Figure 6. A

personalized optical arrangement allows to attenuate the energy of the beam of each harmonic and to propagate them on the same output axis.

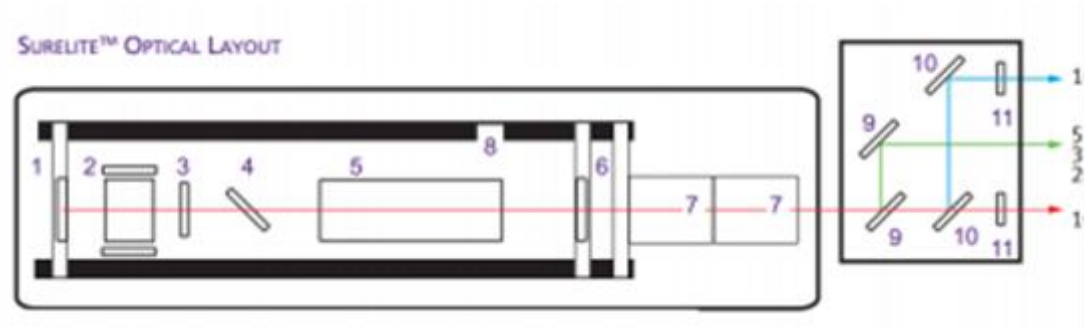

Figure 6. Optical position of the laser ns Nd: YAG (Continuum Surelite III-10)

1. back mirror; **2.** Pockels cell; **3.** Quarter wave plate (λ / 4); **4.** The dielectric polarizer; **5.** Rod Oscillator; **6.** Gaussian output coupling; **7.** Optional harmonic generators; **8.** Graphite resonator; **9.** semi-transparent separating blades; **10.** Mirrors 1064, 532, 355 and 266 *nm*; **11.** Support for blocking the Laser beam.

Obtaining and analyzing the diffraction spectra in the X-rays of GaSb films doped with elements from the iron group

To obtain information about the crystal structure of the films obtained by laser ablation, we used X-ray diffraction (XRD). This technique allows us to analyze different types of materials: samples in bulk, powders or thin films. This type of investigation is based on the interference process of spherical waves generated by atoms periodically arranged in the crystal when a monochromatic beam of X-rays is concentrated on the material. These re-broadcasted waves interfere with each other, constructively or destructively, producing a diffraction picture on a detector. For a constructive interference, the XRD model will present the diffraction lines characteristic of a type of structure. If the used wavelength is close to the inter-atomic distances, the diffraction direction is described by Bragg's formula:

$$2d \sin \theta = n \lambda,$$

where n is an integer and λ is the wavelength of the incident radiation, d is the distance between planes in the atomic network and θ is the angle between the incident radius and scattering plans.

Depending on the geometry of the system, two configurations can be used: $0 \div \theta$ or $0 \div 2\theta$. In the $0 \div \theta$ configuration, the X-ray tube and the detector rotate at an θ angle in relation to the sample surface (which is fix). For the second configuration mentioned, the X-ray tube is fix, while the sample holder and the detector are rotated with θ and 2θ respectively. The geometry used ($0 \div 2\theta$) is called the Bragg-Brentano geometry. Figure 7 shows a schematic representation of this configuration. The phase identification is done by comparing the diffraction patterns obtained experimentally with those recorded in the database. In addition to determining the crystalline structure, by means of this technique other characteristics can also be obtained: quantitative analysis of different phases, study

of phase change, determination of internal stress, etc. For the obtained samples, XRD data were obtained at the University of Craiova, Romania, using a D8-Advance diffractometer (Bruker AXS, Germany) in Bragg-Brentano geometry using CuKα (λ = 0,15405 *nm*, 40 *kV*, 40 *mA*) radiation. The models were registered in the region 5-65 ° 2θ.

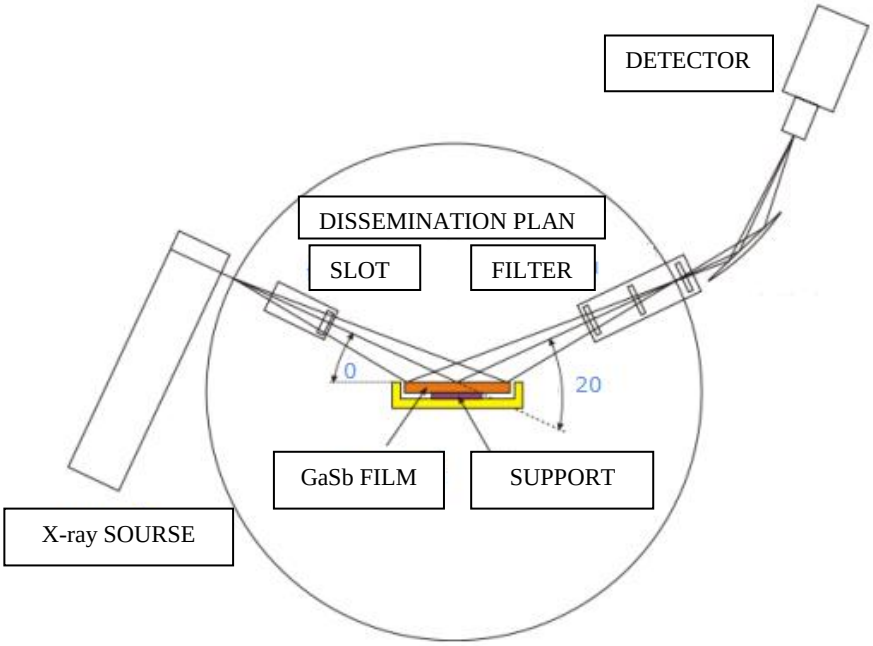

Figure 7. Schematic representation of Bragg-Brentano geometry of the X-ray diffractometer

Figure 7 and 8 shows the diffraction spectra of GaSb (Fe) and GaSb (Mn) films. The recording took place in the angular region 2θ = 20 ÷ 100 degrees. The distances between the interplanes were determined using the Bragg formula.

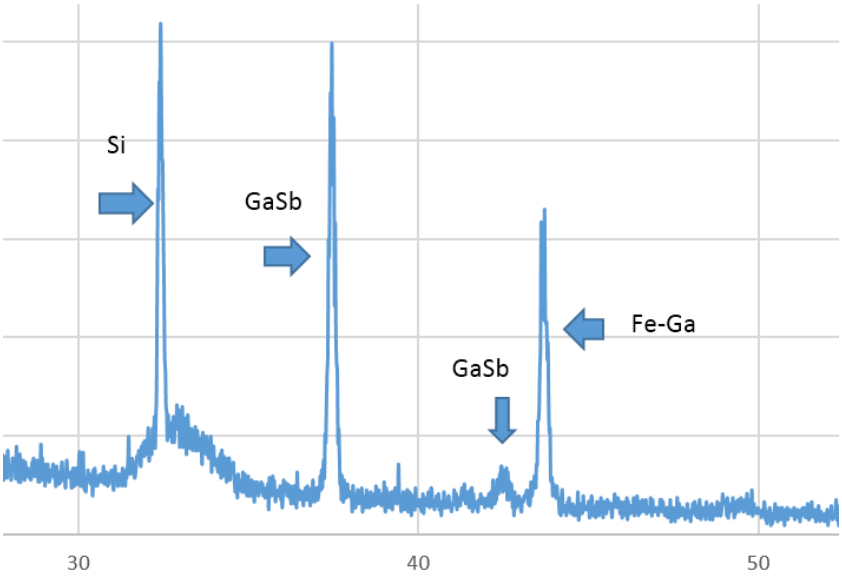

Figure 8. X-ray diffraction spectra from thin films of *GaSb* (0,5%*Fe*)

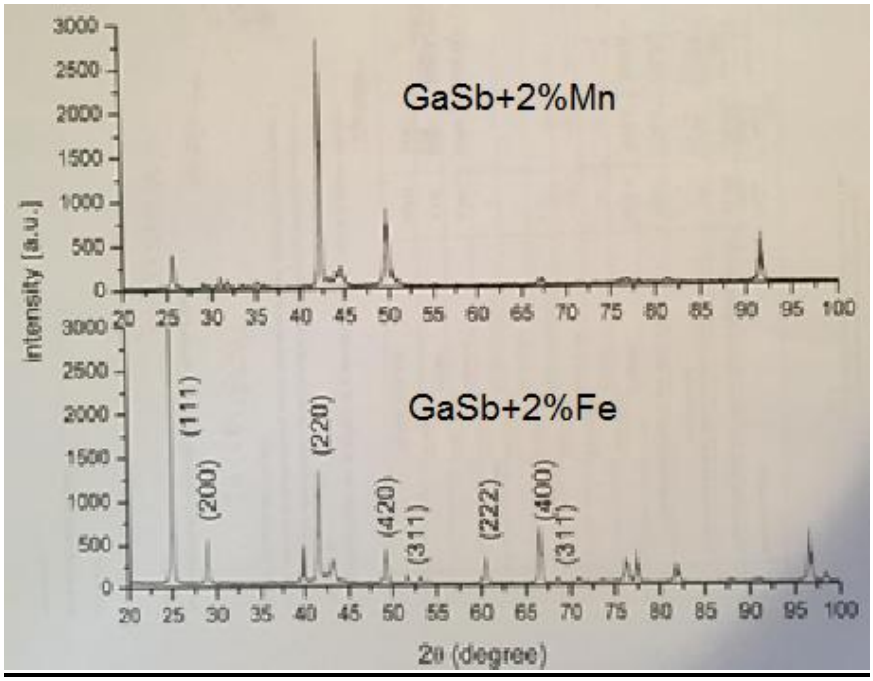

Figure 9. X-ray diffraction spectra from thin films of *GaSb* (*Fe*) and *GaSb* (*Mn*)

The figure shows that the strongest GaSb (Fe) interference lines correspond to angles 25,50; 42,44 degrees. The calculations show that these lines correspond to (111) and (220) plans for the gallium antimony network.

For GaSb (Mn) films, the most intensive interference lines correspond to 42,44 and 50,2 degrees.

It should be taken into consideration that XRD models of thin films do not always resemble those of the bulk material due to their nanostructures and the crystalline nature of the substrate. XRD lines of the nanostructure sample may have different intensity rates or may not be present at all.

The XRD results of the GaSb (Fe) sample showed that two crystalline phases are present: one characterized by the broader peaks and one represented by the narrow diffraction line of the structure. The first mentioned phase may be due to the excess of Sb in this second sample of the excess of Fe.

References

1. Aliyev M.I., Khalilova A.A., Arasly D.H., Rahimov R.N., Tanoglu M., Ozyuzer L. Strain gauges of GaSb-$FeGa_{1.3}$ eutectic composites. In: Appl. Phys.: A, 2004. nr. 79, (8), p. 2075-2079.
2. Allerman A.A., Biefeld R.M., Kurtz S.R.. InAsSb-based mid-infrared lasers (3,8÷3,9 μm) and light-emitting diodes with AlAsSb claddings and semimetal electron injection, grown by metalorganic chemical vapor deposition. In: Applied Phys. Lett., 1996. nr. 69, p. 465-467.

3. Andreev V.M., Sorokina S.V., Timoshina N.K., Khvostikov V.P., Shvarts M.Z. Solar cells based on gallium antimonide. In: FTP, 2006. nr. 40 (10), p. 1275.
4. Bedair S.M., Katsuyama P.K., Chiang N.A., El-Masry M. Tischler, Timmons M. GaAsP-GaInAsSb superlattices: A new structure for electronic devices. In: J. Crystal Growth, 1984. nr. 68, p. 477-482.
5. Benz G., Conradt R. Auger recombination in GaAs and GaSb. In: Phys. Rev. B, 1977. nr. 16, p. 843-855.
6. Bignazzi A., Bosacchi A., Magnanini R. Photoluminescence study of heavy doping effects in Te-doped GaSb. In: J. Applied Phys., 1997. nr. 81, p. 7540-7547.
7. Bougnot G., Paseal F., Roumanille F., Bougnot J., Gouskov L. et al., GaSb and Ga in AsSb photodetectors for lambda-greater-than-1.55 μm prepared by metal organic-chemical vapor-deposition. In: J. Phys., 1988. nr. 49, p. 333-336.
8. Choi H.K., Eglash S.J. High-efficiency high-power GaInAsSb-AlGaAsSb double-heterostructure lasers emitting at 2,3 μm. IEEE. In: J. Quantum Electron., 1991. nr. 27, p. 1555-1559.
9. Cooper C.B., Saxena R.R., Ludowise M.J. The organometallic vapor-phase epitaxy growth of GaSb and $GaAs_{1-x}Sb_x$ using trimethyl antimony. In: J. Electron. Mater, 1982. nr. 11, p. 1001-1010.
10. Dutta P.S., Bhat H.L., Kumar V. The physics and technology of gallium antimonide: An emerging optoelectronic material. In: J. Applied Phys., 1997. nr. 81, p. 5821-5870.
11. Dutta P.S., Sreedhar A.K., Bhat H.L., Dubey G.C., Kumar V., Dieguez E. Current transport properties of metal/hydrogenated amorphous silicon/GaSb structures. In: Applied Phys. Lett., 1995. nr. 67, p. 1001-1003.
12. Esaki L. InAs-GaSb superlattices-synthesized semiconductors and semimetals. In: J. Crystal Growth, 1981. nr. 52, p. 227-240.
13. Fraas L.M., Girard G.R., Avery J.E., Arau B.A., Sundaram V.S., Thompson A.G., Gee J.M. GaSb booster cells for over 30% efficient solar-cell stacks. J. Applied Phys., 1989. nr. 66, p. 3866-3870.
14. Gauneau M., Chaplain R., Rupert A., Toudic Y., Callee R., Andre E. Secondary ion mass spectrometry generates swelling of GaSb: Depth resolution and secondary ion yields. In: J. Applied Phys., 1993. nr. 73, p. 2051-2056.
15. Georgitse E., Gutzuleac L., Mikhelake A., Postolachi I., Yuldashev Sh., Kang T. In: Columbia International Publishing. Journal of Luminescence and Applications. Vol. 1. no.1. p. 1-6. (2014), IF 2,367, ISSN: 0022-2313.
16. Hanson M.P., Driscoll D.C., Zimmerman J.D., Gossard A.C., Brown E.R. Subpicosecond photocarrier lifetimes in GaSb/ErSb nanoparticle superlattices at 1.55 μm. In: Applied Phys. Lett., 2004. nr. 85, p. 3110-3112.

17. Haugan H.J., Szmulowicz F., Brown G.J., Mahalingam K. Optimization of mid-infrared InAs/GaSb type-II superlattices. In: Applied Phys. Lett., 2004. nr. 84, p. 5410-5412.
18. Hildebrand O., Kuebart W., Benz K.W., Pilkuhn M.H. $Ga_{1-x}Al_xSb$ avalanche photodiodes: Resonant impact ionisation with very high ratio of ionisation coefficients. In: IEEE J. Quant. Electron., QE-17, 1981. p. 284-288.
19. Hilsum C., Rees H.D. Three-level oscillator: A new form of transferred-electron device. In: Electron. Lett., 1970. nr. 6, p. 277-278.
20. Kim H., Tarhan E., Chen G., Ramdas A. K., Sciacca M.D., Gunshor R.L. Origin of a localized vibrational mode in a GaSb substrate with a MEE-grown ZnTe epilayer. In: Semiconductor Sci. Technol., 2006. nr. 21, p. 1224-1228.
21. Kindl D., Hubik P., Kristofik J., Mares J.J., Hulicius E. et al. Transport-controlling deep defects in MOVPE grown GaSb. In: Semiconductor Sci. Technol., 2006. nr. 21, p. 180-183.
22. Kluth S.M., Gerald J.D.F., Ridgway M.C. Ion-irradiation-induced porosity in GaSb. In: Applied Phys. Lett., 2006. nr. 86, p.131920-131923.
23. Law H.D., Chin R., Nakano K., Milano R.A. The GaAlAsSb quaternary and GaAlSb ternary alloys and their application to infrared detectors. IEEE J. Quantum Electron., 1981. nr. 17, p. 275-283.
24. Le H.Q., Turner G. W., Eglash S. J., Choi H. K., Coppeta D. A. In: Applied Physics Letters, 1994. nr. 64(2), p. 152-154.
25. Liu F.M., Zhang L.D. X-ray photoelectron spectroscopy of GaSb nanoparticles embedded in SiO_2 matrices by radio-frequency magnetron co-sputtering. In: Semiconductor Sci. Technol., 1999. nr. 14, p. 710-710.
26. Liu Z.Y., Saulys D.A., Kuech T.F. Improved characteristics for Au/n-GaSb Schottky contacts through the use of a nonaqueous sulfide-based passivation. In: Applied Phys. Lett., 2004. nr. 85, p. 4391-4391.
27. Menna R.J., Capewell D.R., Martinelli R.U., York P.K., Enstrom R.E. 3.06 μm InGaAsSb/InPSb diode lasers grown by organometallic vapor-phase epitaxy. In: Applied Phys. Lett., 1991. nr. 59, p. 2127-2129.
28. Merghem K., Teissier R., Aubin G., Monakhov A. M., Ramdane A., Baranov A. N. In: Applied Physics Letters, 2015. nr. 107(11).
29. Morosini M.B.Z., Herrera-Perez J.L., Laural M.S.S., Von Zuben A.A.G., da Silveira A.C.F., Patel N.B. Low-threshold GaInAsSb/GaAlAsSb double-heterostructure lasers grown by LPE. In: IEEE J. Quant. Electron., 1993. nr. 29, p. 2103-2108.
30. Motosugi G., Kagawa T. Temperature dependence of the threshold current of AlGaAsSb/GaSb DH lasers. In: Japanese J. Applied Phys., 1980. nr. 19, p. 2303-2304.

31. Podlecki J., Gouskov L., Pascal F., Pascal-Delannoy F., Giani A. Photodetection at 3.65 μm in the atmospheric window using heteroepitaxy. In: Semiconductor Sci. Technol., 1996. nr. 11, p. 1127-1127.
32. Postolachi I. American Institute of Physics. Proceedings of the physics conference TIM-08. Melville, New-York, 2009. p.92-95.
33. Ricker R. J., Hudson A., Provence S., Norton D. T., Olesberg J. T., Murray L. M., Prineas J. P., Boggess T. F., Ieee J. In: Quantum Elect 51(12), 2015. p. 1-6.
34. Rogalski A., Martyniuk P., Kopytko M. InAs/GaSb type-II superlattice infrared detectors: Future prospect. In: Applied Physics Reviews, 4, 031304 (2017).
35. Segawa K., Miki H., Otsubo M., Shirahata K., Fujibayashi K. Coherent Gunn oscillations in $Ga_{1-x}Sb_x$. In: Electron Lett., 1976. nr. 2, p. 124-125.
36. Su C.H., Su Y.K., Juang F.S. GaSb/InGaSb strained-layer quantum wells by MOCVD. In: Solid-State Electron., 1992. nr. 35, p. 1385-1390.
37. Swaminathan V., Macrander A.T. Materials Aspects of GaAs and InP Based Structures. New Jersey: Prentice Hall, 1991. ISBN-13: 9780133468267. 606 p.
38. Wang C.A., Choi H.K. GainAsSb/AlGaAsSb Multiple-quantum-well diode lasers grown by organometallic vapor phase epitaxy. In: Applied Phys. Lett., 1997. nr. 70, p. 802-802.
39. Wei Y., Gin A, Razeghi M., Brown G.J. Advanced InAs/GaSb superlattice photovoltaic detectors for very long wavelength infrared applications. In: Applied Phys. Lett., 2002. nr. 80, p. 3262-3264.